We are IntechOpen, the world's leading publisher of Open Access books Built by scientists, for scientists

6,900
Open access books available

186,000
International authors and editors

200M
Downloads

154
Countries delivered to

Our authors are among the

TOP 1%
most cited scientists

12.2%
Contributors from top 500 universities

CLARIVATE ANALYTICS
BOOK CITATION INDEX
INDEXED

WEB OF SCIENCE™

Selection of our books indexed in the Book Citation Index
in Web of Science™ Core Collection (BKCI)

Interested in publishing with us?
Contact book.department@intechopen.com

Numbers displayed above are based on latest data collected.
For more information visit www.intechopen.com

Co-Ionic Conduction in Protonic Ceramics of the Solid Solution, BaCe$_{(x)}$Zr$_{(y-x)}$Y$_{(1-y)}$O$_{3-\delta}$ Part II: Co-Ionic Conduction

W. Grover Coors
CoorsTek, Inc
USA

1. Intoduction

BCZY protonic ceramics described in the previous chapter constitute a class of model co-ionic conductors, meaning their transport properties are determined almost exclusively by two ionic species, protons and oxygen ion vacancies. The co-ionic conduction regime is a range of moist atmospheres spanning about 15 orders of magnitude of oxygen pressure, from $10^{-20} < pO_2 < 10^{-5}$ atm., where the total conductivity is independent of oxygen pressure. Evaluation of transport properties in these materials requires new techniques not typically required for traditional ion conductors, or even mixed ionic/electronic conductors. In this chapter, a model for co-ionic conduction, called the CIC model, is proposed that provides both a qualitative and a quantitative understanding of these commercially important ceramic materials. In the last section, the model will be used to deconstruct total conductivity measurements on BCZY27 to obtain partial conductivities as a function of temperature.

Arrhenius analysis is a powerful scientific technique for studying transport properties in ceramic ion conductors. The self-diffusivity of a particular ionic species can be described by,

$$D_i = D^* \exp\left(-\frac{E_a}{k_B T}\right) \tag{1}$$

where D^* is a temperature-independent constant and E_a is the activation energy for migration of the ionic species in the lattice. When log D_i is plotted against reciprorocal temperature, a straight line is obtained where D^* may be found as the y-axis intercept at "infinite" temperature, and E_a may be determined from the slope of the line. Unfortunately, it is often quite difficult to obtain self-diffusivities directly from experiments. Indirect methods are used – most commonly, conductivity measurements, which are easy to make as a function of temperature and surrounding atmosphere. Self-diffusivity and conductivity are related by the well-known Nernst-Einstein relationship,

$$\sigma_i = \left(\frac{z_i^2 F^2 c_i}{RT}\right) D_i \tag{2}$$

It is observed immediately that the proportionality between conductivity and diffusivity involves the concentration of the ionic species. In most cases with ceramic ion conductors, the species concentrations are fixed by a known concentration of extrinsic dopants, which is practically constant over a wide range of operating temperatures, making Arrhenius analysis from conductivity data straightforward and convenient. However, when concentrations of ionic species change appreciably with temperature, traditional Arrhenius analysis is no longer valid. Only in special cases, where the dependence of species concentrations on temperature and pressure is known, can the relationship between conductivity and self-diffusivity be determined. In protonic ceramics, both oxygen ion vacancies and protons are simultaneously present in the lattice, and their respective concentrations depend on the degree of hydration of the host ceramic. Correspondingly, the degree of hydration has a strong dependence on temperature and the surrounding gas atmosphere and can vary spatially throughout the material. However, the respective concentrations of protons and oxygen ion vacancies are not independent. Instead, they are found to change relative to one another in a predictable way. This fixed relationship can be exploited for interpreting conductivity data obtained on protonic ceramic co-ionic conductors and correlating it to species self-diffusivities. Finally, even though many important applications for protonic ceramics are in high pO_2 atmospheres, once the self-diffusivities of protons and oxygen ion vacancies have been determined in the co-ionic regime, the contribution from electronic defects can be inferred by subtraction from the total conductivity at low or high pO_2.

2. Isobaric hydration

The BCZY perovskite ceramics described in Part I contain some compliment of oxygen ion vacancies and electron holes after sintering in air. Y^{3+} ions that substitute on the regular Ce^{+4} and Zr^{+4} B-sites carry an effective negative charge designated by $[Y'_{Ce,Zr}]$ in Kröger-Vink notation. Electroneutrality in the lattice requires charge compensation that results in extrinsic oxygen ion vacancies of double positive effective charge, $[V_O^{\bullet\bullet}]_{extrinsic}$ – one vacancy created for every two substituted dopant ions. A subsequent hydration step is necessary to insert protons into the lattice by means of an exchange reaction with water vapor at the surface of the ceramic. This occurs by the Wagner reaction (Wagner, 1968),

$$H_2O(g) + V_O^{\bullet\bullet} + O_O^{\times} \leftrightarrow 2OH_O^{\bullet} \tag{3}$$

The process of hydration requires the annihilation of an oxygen ion vacancy at the surface (while dehydration requires the creation of an oxygen vacancy). In the process, quasi-free protons are introduced into (or removed from) the oxygen ion sublattice, designated by $[OH_O^{\bullet}]$. Electroneutrality requires that the sum of oxygen vacancies and protons be conservered.

$$2\left[V_O^{\bullet\bullet}\right] + \left[OH_O^{\bullet}\right] = \left[Y'_{Ce,Zr}\right] \tag{4}$$

All of the yttrium ions in this case are assumed to reside only on cerium or zirconium B-sites, and it is equally probable that either Ce^{+4} or Zr^{+4} will otherwise occupy the sites in the solid solution. Although the total concentration of oxygen vacancies and protons is fixed,

Co-Ionic Conduction in Protonic Ceramics of the
Solid Solution, BaCe$_{(x)}$Zr$_{(y-x)}$Y$_{(1-y)}$O$_{3-\delta}$ Part II: Co-Ionic Conduction

503

their relative concentrations may vary, so that an ensemble of two independent mobile ionic species may be present in the ceramic. As straightforward as it may seem, this phenomenon of coexistence of two mobile ionic species in oxide ceramics leads to unusual behavior.

The defect chemistry of protonic ceramics is further complicated by the presence of electronic defects. For example, n-type conductivity may be introduced in very dry atmosphere at low oxygen pressure and high temperatures – a condition not typically encountered where proton conductors are likely to be used. Electron holes, on the other hand, are generated at moderate oxygen pressure by the reaction,

$$\tfrac{1}{2}O_2(g) + V_O^{\bullet\bullet} \rightarrow O_O^{\times} + 2h^{\bullet} \tag{5}$$

These holes may subsequently be annihilated by water vapor by the reaction,

$$H_2O(g) + 2h^{\bullet} + 2O_O^{\times} \rightarrow \tfrac{1}{2}O_2(g) + 2OH_O^{\bullet} \tag{6}$$
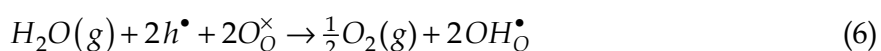
The summation of Eq. 5 and Eq. 6 gives Eq. 3, and it is possible (and perhaps, likely) that Wagner hydration actually occurs by this two-step process. Not all ceramic oxides with oxygen vacancies undergo Wagner hydration. In fact, the phenomenon seems to be restricted to a relatively small group of ceramics, possibly pointing to the important role played by holes in the overall hydration process. Recently, Yoo and colleagues (Yoo, et al. 2009) have proposed that holes play a fundamental role in the transient behaviour of hydration in protonic ceramics upon sudden changes in pH$_2$O. However, since holes are created and subsequently annihilated, their concentration at equilibrium is low in moist atmosphere at intermediate oxygen pressure (pO$_2$ < 10^{-5} atm). For this reason, by assuming equilibrium under fixed water vapor pressure, the contribution of electronic defects to total conductivity may generally be neglected at equilibrium. On the other hand, holes are expected to contribute to ambipolar diffusion at higher pO$_2$. A comprehensive theory for multi-species transport in ceramic proton conductors was originally proposed by Tan (Tan et al., 2000) and more recently expanded by Sanders (Sanders & O'Hayre, 2009).

The CIC model only applies in the ionic regime of the Kröger-Vink diagram where defect concentrations are independent of oxygen pressure. Wagner hydration occurs by Eq. 3, where hydration and dehydration at equilibrium depend on temperature and water vapor partial pressure as well as the concentration of oxygen ion vacancies at the surface according to the mass action law,

$$K_{eq} = \frac{\left[OH_O^{\bullet}\right]^2}{p_{H_2O}\left[O_O^{\times}\right]\left[V_O^{\bullet\bullet}\right]} \tag{7}$$

The usual thermodynamic meaning applies,

$$-RT\ln K_{eq} = \Delta G = \Delta H - T\Delta S \tag{8}$$

Brackets refer to mole fractions. Molar concentrations are obtained by dividing by the molar volume. In the crystalline lattice, oxygen ion sites are conserved so the molar volume V_m is equivalent to N_a times the unit cell volume V_c of the cubic ABO$_3$ perovskite. The fraction of extrinsic oxygen vacancies "stuffed" by water molecules is defined as the extent of

hydration, Chi (χ), where $0 < \chi < 1$. Two protons are generated for each oxygen vacancy "stuffed", and there are two dopant ions required for every oxygen ion vacancy.

$$\chi = \frac{[H_2O]}{\left[V_{O,extrinsic}^{\bullet\bullet}\right]} = \frac{\left[OH_O^{\bullet}\right]}{\left[Y_{Ce,Zr}'\right]} \quad ; 0 \leq \chi \leq 1 \tag{9}$$

At equilibrium, the extent of hydration, χ, is a strong function of temperature and water vapor pressure. Its value may be calculated using the formula derived by Kreuer, obtained by inserting the O-site conservation and electroneutrality condition into Eq. 7 (Kreuer, 1999).

$$\chi = \frac{3K - \sqrt{K(9K - 6KS + KS^2 + 24S - 4S^2)}}{(K-4)S} \tag{10}$$

$K \equiv K_{eq}p_{H_2O}$. The partial pressure of water vapor p_{H_2O} is at the gas/solid interface and K_{eq} is the equilibrium constant for Eq. 3. (If hydration occurs by the two step process of Eq. 5 and Eq. 6, then $K_{eq} = K_{eq,5} K_{eq,6}$). The constant S is the fraction of dopant ions per formula unit, equal to $\left[Y_{Ce,Zr}'\right]$ in the absence of electronic defects or A-site substitution. For BCZY doped with 10 mol% yttria, S = 0.1. When χ is plotted as a function of temperature, a sigmoidal curve is produced. At high temperatures the ceramic becomes dehydrated ($\chi \to 0$), and at low temperatures, the hydration is "frozen in" at the hydration limit ($\chi \to 1$). This is an idealization since, as a practical matter, the limits of total hydration and dehydration are not thermodynamically achievable. Some residual vacancies and some residual hydration will always be present. The value of χ as a function of temperature may be determined experimentally by either isobaric thermogravimetry or dilatometry. Alternatively, it may be determined by curve fitting of total conductivity data. This latter technique has been explored with some success on rare earth calcium-doped niobates by Haugsrud (Haugsrud & Norby, 2006).

3. Partial conductivities

Extent of hydration is related to defect concentrations in units of mol/cm³ by,

$$c_{OH_O^{\bullet}} = \frac{S}{V_m}\chi \quad ; \quad c_{V_O^{\bullet\bullet}} = \frac{S}{V_m}\frac{(1-\chi)}{2} \tag{11}$$

Substituting the concentrations from Eq. 11 into the Nernst-Einstein relationship (remembering that z^2 is 1 for protons and 4 for oxygen ion vacancies) leads to the partial conductivities,

$$\sigma_{OH_O^{\bullet}} = \left(\frac{1}{T}\right)\beta\chi D_{OH}^{\circ}\exp\left(-\frac{E_{a,OH}}{k_BT}\right) \tag{12}$$

$$\sigma_{V_O^{\bullet\bullet}} = \left(\frac{1}{T}\right)\beta 2(1-\chi)D_V^{\circ}\exp\left(-\frac{E_{a,Vo}}{k_BT}\right) \tag{13}$$

Co-Ionic Conduction in Protonic Ceramics of the
Solid Solution, BaCe$_{(x)}$Zr$_{(y-x)}$Y$_{(1-y)}$O$_{3-\delta}$ Part II: Co-Ionic Conduction

505

D_{OH}° and D_{V}° [cm²/s] are temperature independent, pre-exponential self-diffusion coefficients, and $E_{a,OH}$ and $E_{a,Vo}$ are the corresponding activation energies for migration. β is a constant for a given ceramic material evaluated as,

$$\beta = \frac{F^2 S}{R V_m} = \frac{e^2 S}{k_B V_c} \left[\frac{Ks}{\Omega cm^3} \right] \qquad (14)$$

where F is Faraday's constant, R is the universal gas constant, e is the elementary charge, k_B is Boltzmann's constant, V_m is the molar volume, and V_c is the cubic ABO$_3$ unit cell volume in cm³. It is observed that the dimensionality of β is consistent so that when multiplied by D/T, in units of cm²/K.s, the proper units of conductivity, $(\Omega\ cm)^{-1}$, are obtained.

The co-ionic conduction model treats the total conductivity as the sum of only the two ionic species.

$$\sigma_{tot} = \sigma_{OH_O^{\bullet}} + \sigma_{V_O^{\bullet\bullet}} \qquad (15)$$

By combining partial conductivities (Eq. 12 and 13), an important linear relationship between σ_{tot} and χ is found,

$$\sigma_{tot} T = \beta \chi \left(D_{OH_O^{\bullet}} - 2D_{V_O^{\bullet\bullet}} \right) + 2\beta D_{V_O^{\bullet\bullet}} \qquad (16)$$

In the limit of complete hydration, the total conductivity is equal to the proton conductivity, and in the limit of complete dehydration, the total conductivity is equal to the oxygen ion vacancy conductivity. At intermediate extent of hydration, the total conductivity reflects the ionic species ensemble. χ is constant at steady state once equilibrium with the surrounding atmosphere is reached. Under transient conditions, such as when temperature and water vapor pressure change or a water vapour pressure gradient is imposed, χ is a local variable that depends on position and time within the ceramic. Using Eq. 16, it is possible to determine the partial conductivities from total conductivity measurements if extent of hydration is known as a function of temperature. The determination of partial conductivities of protons and oxygen ion vacancies and proton transference number is important for electrochemical applications such as protonic ceramic fuel cells, steam electrolyzers, and hydrogen separation membranes; but it is also important for steam permeable membranes (Coors, 2007) since one important consequence of having two, independent, mobile ionic species is the possibility of ambipolar water diffusion.

It is necessary to stress an important point about applying the Nernst-Einstein equation to an ensemble of mobile ionic species by the preceding derivation. Equations 12 and 13 imply that protons and oxygen ion vacancies may diffuse independently. In the conductivity experiment this condition is met by using electrodes that are reversible to both species, which requires electrochemical redox reactions at the surface for both hydrogen and oxygen independently. However, the Wagner reaction (Eq. 3) is not an electrochemical redox reaction. That is, no electrons flow into an external circuit, and electrodes are, therefore, not required for hydration and dehydration. The Wagner reaction only describes the chemical interaction of the ceramic with water vapor and the relative defect concentrations that ensue. In the absence of electrodes, Eq. 16 still applies, as diffusion is constrained by electroneutrality resulting in chemical diffusion of water, but the partial conductivities are no longer defined by electrode potentials.

The protonic transference number is defined as,

$$t_{proton} \equiv \frac{\sigma_{OH_O^\bullet}}{\sigma_{OH_O^\bullet} + \sigma_{V_O^{\bullet\bullet}}} = \frac{1}{1 + \dfrac{2(1-\chi)}{\chi}\left(\dfrac{D_V}{D_{OH}}\right)} \qquad (17)$$

Protonic transference number, it is observed, is not a constant, but a function of concentration - that is, the extent of hydration. Extent of hydration (Eq. 10) and proton transference number (Eq. 17) both have the same sigmoidal functional form. In fact, it may be seen for the special case where the self-diffusivity of oxygen ion vacancies is exactly half that of proton diffusivity, $D_V / D_{OH} = \dfrac{1}{2}$, that t_{proton} is identical to χ.

The co-ionic conduction model is highly idealized, containing several fundamental underlying assumptions:

1. Conduction due to electrons and holes is neglected. This assumption is valid under moist atmosphere as long as the temperature and oxygen pressure are not too high or too low.

2. Mobile $OH_O^\bullet$ and $V_O^{\bullet\bullet}$ defects each have a single, temperature-independent pre-exponential diffusion constant and activation energy, which is also independent of atmosphere. Strictly speaking, this assumption is valid only at equilibrium in the dilute limit, where the concentration of defects is low enough so that they do not interact with one another. Also, the crystal lattice is known to expand when protonic ceramics hydrate, causing a change in migration enthalpy. This effect has been neglected in the present model.

3. The total concentration of $OH_O^\bullet$ plus $V_O^{\bullet\bullet}$ is fixed by the extrinsic dopant concentration. Furthermore, all dopant ions are assumed to reside exclusively on B-sites in the ABO_3 perovskite.

4. Extent of hydration χ, is a temperature- and water vapor pressure-dependent variable that is determined by an equilibrium constant for hydration with a constant value of enthalpy and entropy. $\left[OH_O^\bullet\right] \propto \chi$ and $\left[V_O^{\bullet\bullet}\right] \propto (1-\chi)$

With these four assumptions, it is possible to develop a useful analytical model that yields further insight into co-ionic conduction. Despite its apparent simplicity, the model is deceptively complex due to the exponential terms, which make routine algebraic evaluation impossible. Fortunately, the execution of the model can be carried out with ease in a spreadsheet like Microsoft Excel.

4. Hydration and dehydration

Co-ionic conduction is obviously only possible when protons and oxygen vacancies co-exist in the lattice. At equilibrium, the Wagner reaction is assumed to be thermodynamically reversible, so that at constant water vapor pressure, the ratio of protons to oxygen vacancies depends only on temperature. If no hydration were to occur, only oxygen vacancies would be present and the material would behave just like an ordinary oxygen ion conductor. If dehydration did not occur - that is, if hydrogen, rather than water vapor, could enter the lattice directly by a different mechanism - proton conduction would prevail at all

Co-Ionic Conduction in Protonic Ceramics of the
Solid Solution, $BaCe_{(x)}Zr_{(y-x)}Y_{(1-y)}O_{3-\delta}$ Part II: Co-Ionic Conduction
507

temperatures. Defect reactions of this type are only possible in very dry hydrogen in ceramic proton conductors or, as pointed out by Tan (Tan, et al. 2000) mixed proton-hole conduction is possible when a pO_2 concentration gradient is present.

The details of how the ratio of protons to oxygen vacancies changes with temperature are captured in Kreuer's formula for isobaric degree of hydration. From Eq. 10 it may be shown that hydration achieves a saturation value at low temperatures, where the protonic defect concentration is frozen in, i.e. $\chi \to 1$ as $T \to 0$. Eq. 10 also requires that $\chi \to 0$ as $T \to \infty$. Complete dehydration in these materials typically occurs below 1200 °C, but there is no fundamental requirement for total dehydration to take place below the melting point. This equation generates a sigmoidal plot versus temperature with a characteristic inflection at the mid-point. The temperature at the inflection point, T_c, is a strong function of hydration enthalpy. Figure 1 shows plots of Eq. 10 at $pH_2O = 0.025$ atm for three different hydration enthalpies ($\Delta H = -80, -100,$ and -120 kJ/mol) at constant entropy ($\Delta S = -120$ J/mol.K). It may be seen that a change in ΔH of only 40 kJ/mol causes a 400 °C translation of T_c. The slope of the curve in the transition region is determined by the hydration entropy. Figure 2 shows this effect for $\Delta S = -80, -120,$ and -160 J/mol.K, where the enthalpy has been adjusted so that each curve has the same inflection point. It is observed that the hydration/dehydration transition becomes more abrupt as the reaction entropy becomes more negative, but the effect is not nearly as pronounced as for different enthalpies.

Total conductivity vs. temperature measurements of ceramic proton conductors are routinely made and reported in the literature, but often with little underlying recognition of the consequences of co-ionic conduction. This has resulted in confusion in interpretation of Arrhenius plots. Only recently has it become more widely recognized that there is a requirement for deconvolving partial conductivities from the total conductivity data. This can be a formidable challenge. Looking at Eqs. 12 and 13 it may be observed that these coupled equations contain one common unknown variable, χ, and two decoupled unknown parameters for each species - the pre-exponentials and migration activation energies. At low temperature, in moist atmosphere, it is generally valid to assume that the total conductivity is due to protonic conduction alone (Eq. 12). Thus, the bulk protonic activation energy, $E_{a,OH}$, may be immediately determined from the slope of the Arrhenius conductivity plot at low temperature. The pre-exponential D_{OH}, however, cannot be determined from the extrapolation of the low temperature plot to the y-axis, as is usually done with single-ion conduction data, without knowing the terminal hydration limit, χ as $T \to 0$. Variations in this value will shift the low temperature portion of the curve up and down, moving the intercept. At high temperatures in dry atmosphere, it is often safe to assume that conduction is due to oxygen vacancies alone (Eq. 13). In this case, the activation energy, $E_{a,Vo}$, may be determined by the slope. The pre-exponential, D_{Vo}, may be determined by the y-intercept of the extrapolation of the high temperature portion of the curve since, in this case, it may also be generally assumed that the ceramic is essentially dehydrated so that $\chi \approx 0$. However, caution must be exercised if either the hydration enthalpy is strongly negative or the entropy is not too negative, as evident from Figure 1. Once the self-diffusivities of protons and oxygen ion vacancies are determined at the high and low temperature extremes, the portion of the conductivity plot at intermediate temperatures, where χ is variable, must provide a smooth transition that obeys Eq. 16 at all temperatures. This reflects the fact that the species partial conductivities are not constant. The total conductivity is the sum of the two partial conductivities at a given temperature. The important features are apparent at intermediate temperatures, where proton conductivity reaches a maximum before dropping at higher temperatures due to dehydration, and oxygen vacancy conduction begins to

dominate. The oxygen ion vacancy partial conductivity curve is characterized by a "dog leg" caused by an increase in oxygen vacancy concentration due to dehydration. The sum of the two curves produces the characteristic "crook" often observed in conductivity plots of these materials. Many examples of co-ionic conduction are seen in the literature exhibiting this hydration/dehydration "crook". A good example is shown in Fig. 16 of Kreuer's 2003 review on Proton-Conducting Oxides (Kreuer, 2003), where this behavior is clearly visible in the total conductivity portion of each of the plots. The co-ionic conductivity model provides a good qualitative understanding of this phenomenon.
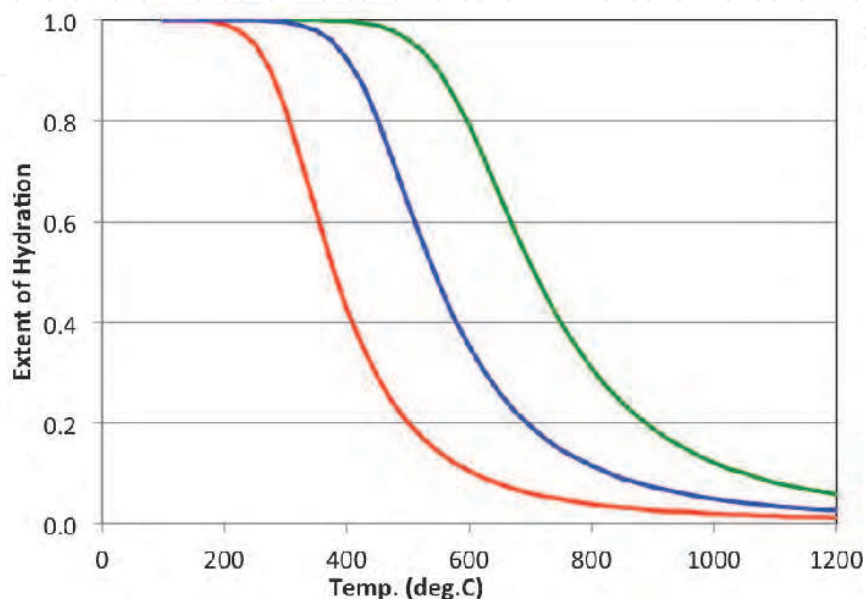
Fig. 1. Extent of hydration vs. temperature by Eq. 10 (isobaric p_{H2O} = 0.025 atm). ΔH = -80 (red), -100 (blue), -120 (green) kJ/mol, with constant ΔS = -120 J/mol.K.
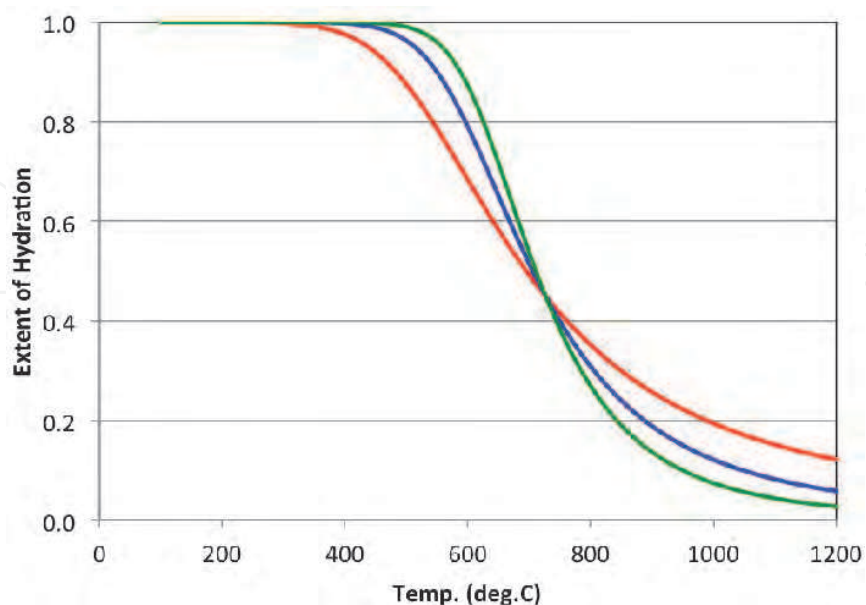
Fig. 2. Extent of hydration vs. temperature by Eq. 10 (isobaric p_{H2O} = 0.025 atm). ΔS [J/mol.K], ΔH [kJ/mol] = -80, -80 (red), -120, -120 (blue), -160, -160 (green).

Co-Ionic Conduction in Protonic Ceramics of the
Solid Solution, BaCe$_{(x)}$Zr$_{(y-x)}$Y$_{(1-y)}$O$_{3-\delta}$ Part II: Co-Ionic Conduction

509

5. Ambipolar diffusion

Ambipolar diffusion occurs in the co-ionic ensemble with chemical diffusivity derived by Kreuer (Kreuer, 1999).

$$\tilde{D}_{H_2O} = \frac{(2-\chi)D_{OH_O^{\bullet}}D_{V_O^{\bullet\bullet}}}{\chi D_{OH_O^{\bullet}} + 2(1-\chi)D_{V_O^{\bullet\bullet}}} \tag{18}$$

$D_{OH_O^{\bullet}} = D_{OH}^* \exp\left(-E_{a,OH}/k_BT\right)$ and $D_{V_O^{\bullet\bullet}} = D_V^* \exp\left(-E_{a,V}/k_BT\right)$ where D_{OH}^* and D_V^* are the temperature independent, pre-exponential self-diffusion coefficients [cm²/s], and $E_{a,OH}$ and $E_{a,Vo}$ are the corresponding activation energies for migration of protons and oxygen ion vacancies, respectively. It is interesting to consider the derivative of the chemical diffusivity with respect to extent of hydration,

$$\frac{d\tilde{D}_{H_2O}}{d\chi} = \frac{-2D_{OH_O^{\bullet}}D_{V_O^{\bullet\bullet}}\left(D_{OH_O^{\bullet}} - D_{V_O^{\bullet\bullet}}\right)}{\left[\chi D_{OH_O^{\bullet}} - 2D_{V_O^{\bullet\bullet}}(1-\chi)\right]^2} \tag{19}$$

Surprisingly, this derivative has no roots. So, unlike proton conductivity, there is no value of χ between 0 and 1 that produces a maximum in chemical diffusivity. This unusual behavior results from the exact cancellation of all terms containing χ in the numerator, and shows that ambipolar diffusion must increase monotonically with temperature.

It is seen in Eq. 11 that χ and concentration are proportional, making it possible to cast Fick's 2nd Law in the more convenient dimensionless variable, χ which has implicit dependency on time and space variables, $\chi = \chi(r,t)$.

$$\frac{\partial \chi}{\partial t} = \nabla\left(\tilde{D}_{H_2O}(\chi)\nabla \chi\right) \tag{20}$$

Eq. 20 must be solved numerically because the spatial derivatives of Eq. 18 result in nonlinear coefficients. At steady state, the concentration gradient is stationary, and Eq. 20 may be integrated to give the spatial dependence of $\tilde{D}_{H_2O}$ across the membrane. In the absence of an externally applied electrical potential, the effective steam permeation flux (in units of mol/cm2.s) may be found.

$$J_{H_2O} = -\tilde{D}_{H_2O}(c)\nabla c = -\frac{S}{2V_m\Delta x}\int_{\chi_1}^{\chi_2}\frac{(2-\chi)D_{OH_O^{\bullet}}D_{V_O^{\bullet\bullet}}}{\chi D_{OH_O^{\bullet}} + 2(1-\chi)D_{V_O^{\bullet\bullet}}}d\chi \tag{21}$$

In one dimension, Δx is the electrolyte membrane thickness and $dc(H_2O) = (S/2V_m)d\chi$. χ_1 and χ_2 are the extent of hydration at the respective gas/solid interfaces of the membrane ($\chi_2 \geq \chi_1$). The concentration of dopant ions is proportional to the proton concentration, but two protons make one effective "water" in the lattice – thus, the additional factor of 2 in the denominator. Eq. 21 may be solved analytically (the complete solution may be found in (Coors, 2004)), but a much more intuitive form may be obtained if partial conductivities are substituted for partial diffusivities. This is only strictly valid for the case of uniform

temperature and where the steam gradient is small. This simplification permits the partial conductivities to be moved out of the integral and mathematically separates conductivity from extent of hydration. The result is given in Eq. 22 and 23.

$$J_{H_2O} = -\frac{RT}{4F^2\Delta x}\left(\frac{\sigma_{OH}\sigma_{Vo}}{\sigma_{OH}+\sigma_{Vo}}\right)\int_{\chi_1}^{\chi_2}\frac{(2-\chi)}{\chi(1-\chi)}d\chi \qquad (22)$$

$$J_{H_2O} = -\frac{RT}{4F^2\Delta x}\left(\frac{\sigma_{OH}\sigma_{Vo}}{\sigma_{OH}+\sigma_{Vo}}\right)\ln\left[\frac{\chi_2^2(1-\chi_1)}{\chi_1^2(1-\chi_2)}\right]; \quad (0<\chi<1) \qquad (23)$$

As can be seen by this simplification, the steam flux only depends on the extent of hydration at the interfaces. The term containing the partial conductivities in Eq. 23 is characteristic of ambipolar diffusion. It is equivalent to $\sigma_{Vo}t_{proton}$. It may be observed that the magnitude of the flux is determined by the partial conductivity with the smaller value – generally the oxygen ion vacancy conductivity. The following logarithmic term, however, is peculiar to the behavior of steam permeable membranes. This term is an enhancement factor that is dominated by the square of the ratio of the extent of hydration at the interfaces. This serves to greatly enhance the steam flux beyond what would normally be expected. For example, with χ on the moist side equal 0.5 and χ on the dry side equal to 0.002, a steam flux enhancement of more than ten times is predicted. This is an important consideration when the dry side contains hydrocarbon species, because any steam that permeates will be quickly consumed. Although the steam permeation flux is generally small – on the order of 10 nmol/cm^2.s for typical values of the partial conductivities at 700 ^{o}C – the enhancement factor has the potential to boost the steam flux significantly.

6. Electrical characterization

6.1 Introduction

A co-ionic conduction model for protons and oxygen ion vacancies in protonic ceramic perovskites was presented in the previous section. Even in its most simplified form, six fitting parameters are still required: two self-diffusivity pre-exponentials, two migration activation energies, and hydration enthalpy and entropy. In this section a fitting procedure, based on isobaric, steady-state conductivity analysis over a wide temperature range is used for determining these parameters with experimental data for the proton conductor, BCZY27.

6.2 Conductivity experiments

The experiments for measuring conductivity and diffusivity are generally not the same. The distinction is subtle, and often leads to errors in interpreting experimental data. Conductivity measurements require electrodes and the measurement of the electrochemical potential gradient. On the other hand, hydration and dehydration occur by ambipolar diffusion, which does not require electrodes. The conductivity experiment generally presupposes a uniform, steady-state concentration of mobile defect species. Electrodes, reversible to hydrogen and electrons, provide an alternative way for protons to enter the lattice, perturbing the defect equilibrium in unanticipated ways. Generally specimens used

Co-Ionic Conduction in Protonic Ceramics of the
Solid Solution, BaCe$_{(x)}$Zr$_{(y-x)}$Y$_{(1-y)}$O$_{3-\delta}$ Part II: Co-Ionic Conduction

511

for conductivity measurements have large area, planar electrodes separated by a relatively thin specimen. Under well-equilibrated test conditions, in a balanced cell arrangement, with uniform atmosphere at each electrode, proton or mixed proton/hole conductivity may be measured once the extent of hydration reaches a steady-state value. For unbalanced cells with different water vapor or hydrogen pressure at each electrode, the measurement is no longer valid since a constant flux of steam is induced. Specifically, the Nernst potential cannot be used to determine the protonic transference number in this case as proposed by Norby (Norby, 1988; Sutija, et al., 1995).

For conductivity measurements of the co-ionic ensemble in ceramic proton conductors, electrodes must be placed so as not to perturb the defect concentrations. This has been accomplished in the present experiments by using a long, rod with circumferential electrodes placed at each end. This rod has a large surface area for optimal surface exchange with gaseous species, and a relatively small electrode area. Most importantly, diffusion occurs in the radial direction, and conductivity is measured in the axial direction – the direction of the electric field lines required for the conductivity measurement. This means that the conductance instrument measures the arithmetic mean conductance of the rod (Maier, 2004, p.229),

$$R^{-1} = \frac{2\pi}{L} \int_{r=0}^{r=R_b} \sigma(r) \, r \, dr \tag{24}$$

where R is the measured specimen resistance. Eq. 24 is valid as long as the conductivity depends only on the radial, and not the axial (z-axis), position along the length of the rod between the electrodes. Previously it was shown,

$$\sigma_{tot} T = \beta \chi \left(D_{OH_O^\bullet} - 2D_{V_O^{\bullet\bullet}} \right) + 2\beta D_{V_O^{\bullet\bullet}} \tag{16}$$

Inserting Eq. 16 into Eq. 24 provides the necessary bridge between the conductivity and diffusion experiments.

$$R^{-1} = \frac{2\pi\beta}{TL} \int_{r=0}^{r=R_b} \left[\left(D_{OH_O^\bullet} - 2D_{V_O^{\bullet\bullet}} \right) \chi(r) + 2\beta D_{V_O^{\bullet\bullet}} \right] r \, dr \tag{25}$$

Of course, $\chi(r, t)$ is not generally known except at steady-state. It must be determined by solving the diffusion equation (Eq. 20) subject to boundary and initial conditions,

$$\begin{aligned}
\chi(R_b, t > 0) &= \chi^\circ \\
\chi(r, t = 0) &= \chi_i \\
\chi(r, t \to \infty) &= \chi^\circ
\end{aligned} \tag{26}$$

The measurement of conductivity can only sense the mean conductivity of all the mobile species in the cross-section of the specimen between the electrodes. The concentration of defects may or may not be uniform depending on whether or not the specimen has reached thermodynamic equilibrium with the surrounding atmosphere. The important feature of the experiments described herein is that the partial conductivities of individual species may be extracted from the diffusion experiment because diffusion and migration are orthogonal –

diffusion is perpendicular to free surfaces (radial) and migration is perpendicular to the electrodes (axial). Direct current measurements cannot be employed here because the defects would become polarized in the axial direction. Low frequency a.c. is necessary so that, even though the charged defects oscillate back and forth in the axial direction, their average concentration does not change as long as the mean free path is short compared to the length of the specimen.

Isobaric conductivity measurements are made under constant p_{H_2O} and p_{H_2} atmosphere by changing temperature slowly enough to maintain defect equilibrium over the entire range of temperatures. Also, $\chi(T, p_{H_2O})$ must be known, which means that either $\Delta G^\circ(T, p_{H_2O})$ for hydration must be known in advance, or ΔG° must be determined empirically by fitting isobaric conductivity vs. temperature data. In this method, $D_{OH_O^\bullet}$ is determined by Arrhenius analysis of conductivity in the hydration limit ($\chi \to 1$) at low temperature and $D_{V_O^{\bullet\bullet}}$ in the dehydration limit ($\chi \to 0$) at high temperature, and fitting the conductivity measurements at intermediate temperatures to the CIC model.

6.3 Specimen preparation

The fabrication and microstructure of the protonic ceramic, BCZY, was presented in Part I. For the conductivity measurements, an extruded rod of 2NiBCZY27, 3.36 mm diameter was used. The rod was cut to a length of 4 cm. A platinum wire was wrapped around each end and twisted into a pigtail. A band of platinum paste (ESL 5524) was painted on each end and covering the wires. The platinum paste and leads were sintered at 975 °C for 15 minutes in air. The distance between electrodes was 3.45 cm, giving a resistance cross-section (A/t) of 0.0257 cm.

6.4 Test apparatus

All conductivity measurements were carried out in a sealed, 5 cm diameter alumina ceramic process tube in a horizontal tube furnace (Thermolyne 21100). Four platinum wires extended to the specimen through gas-tight feedthroughs for connection to the measuring instruments outside the furnace. Two Pt lead wires were attached to each pigtail on the specimen for 4-point measurements, and a type-K thermocouple was mounted about 1 cm from the specimen. Process gas was introduced at a flow rate of 100 ml/min about 1 cm upstream of the specimen, and an in-situ zirconia oxygen sensor tube (CoorsTek Pt-ZDY4), referenced to ambient air with a second intergral type-K thermocouple, was positioned about 5 cm downstream of the specimen to give very rapid and sensitive response to changes in local p_{O_2}. Gas flowed out of the far end of the process tube through a bubbler. Outlet flow calibration was obtained using a flow-rate bubble meter.

Moist and dry 4% H$_2$-bal Ar gases were prepared by splitting the flow from the gas cylinder from a common manifold through two precision needle valves. One stream passed through a chromatography drying column (CRS Big Trap) and the second stream passed through a water bubbler at room temperature. The moist and dry streams were then connected to the two inlet ports of a 2-position, 4-way ball valve. Whenever the valve position was switched, the selected output flowed into the furnace and the non-selected output exhausted into room. This way, each gas steam continued flowing at steady-state regardless of valve position, without any build up of back pressure that would otherwise occur if one of the streams was stopped while the other was flowing. With the 4-way valve configuration no pressure transients were introduced when the process gas was switched between the moist and dry condition.

Co-Ionic Conduction in Protonic Ceramics of the
Solid Solution, BaCe$_{(x)}$Zr$_{(y-x)}$Y$_{(1-y)}$O$_{3-\delta}$ Part II: Co-Ionic Conduction

513

6.5 Resistance measurement

The resistance of the specimen was measured using an Agilent 4338B Precision Miliohmmeter. This instrument provides 4-probe resistance measurements at a fixed frequency of 1000 Hz, which is a good frequency for this type of experiment because the frequency is high enough to eliminate noise and polarizations due to electrodes, contact potentials and thermoelectric effects while still capturing the true bulk resistance of the specimen. The 4338B generates a single pair (real and imaginary) of impedance data at each measurement. As long as the reactance value is much less than the real resistance, the measurements can be considered to be representative of the true bulk specimen resistance. Of course, the fixed frequency measurement does not afford the detailed analysis of impedance spectroscopy, such as grain vs. grain boundary conductance. A Hewlett Packard 4195A Network analyzer operating between 10 Hz and 5 MHz was also used periodically to confirm that the measurement at 1000 Hz was representative of the bulk conductance. Since the total electrode area was small, electrode impedance effects were negligible. At high temperatures, features of impedance spectra were difficult to resolve, and no significant difference between the "bulk" resistance and the resistance at 1000 Hz was observed. Above 400 °C, where most of the measurements were made, no grain boundary arcs were visible in the spectra and only a single bulk arc was present above 1000 Hz. At intermediate temperatures, where impedance spectroscopy is often useful, the arcs resulting from mixed protons and oxygen ion vacancies overlap, making attempts to resolve impedance arcs separately virtually meaningless in the range of temperatures where the partial conductivities are about the same order of magnitude. Again, fixed frequency measurements proved to be a good compromise and considerably more convenient from the standpoint of the enormous amount of data generated during temperature scans lasting several days in some cases. Because of the large ratio of cross-sectional area to length in the rod specimens, resistance values ranged from about 5000 Ω at the highest temperatures to about 150 kΩ at the lowest temperatures. With such large resistance values, there was no concern about the instrument input impedance as often plagues the measurements of thin specimens that can typically be in the milliohm range.

Resistance measurements, thermocouple readings, and O$_2$ sensor voltages were continuously logged using a data acquisition computer running in the LabView environment. The complete test apparatus is shown in Figure 3.
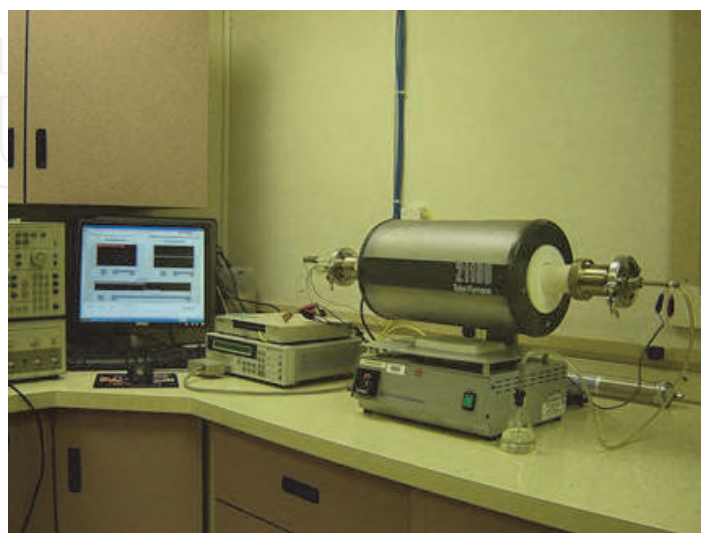

Fig. 3. Conductivity test apparatus

6.6 pH$_2$O determination

The extent of hydration, as determined by Eq. 10, depends strongly on the water vapour pressure at the surface of the specimen. A common mistake that is made in experiments for evaluating ceramic proton conductors is to assume that the p_{H_2O} inside the processes vessel is the same as the saturated pressure at the bubbler used to moisten the process gas. Since both hydrogen and water vapour are exchanged with the ceramic specimen, it is not correct to assume that p_{H_2O} is invariant, and it needs to be measured along with temperature and conductivity. This can be done with an external dew point monitor, but also with an in-situ oxygen sensor, which is mounted in close proximity to the test specimen. The oxygen pressure is determined from the Nernst voltage by,

$$P_{O_2} = P_{O_2,ref} \exp\left(-\frac{4FV_N}{RT}\right) \tag{27}$$

where F is Faraday's constant, R is the universal gas constant and T is absolute temperature. The reference oxygen pressure in this case is ambient air, 0.2095 atm, adjusted for Salt Lake City, Utah, (0.858atm/atm), or 0.180 atm. The ratio of water vapour pressure to hydrogen pressure is determined by the oxygen sensor,

$$\frac{P_{H_2O}}{P_{H_2}} = K_w \sqrt{P_{O_2}} \tag{28}$$

where K_w is the temperature-dependent equilibrium constant for water formation evaluated by the empirical relationship (JANAF),

$$\Delta G_f^o = -RT \ln K_w = (-57.031 + 2.799x10^{-3}T\ln T \\ -0.576x10^{-6}T^2 + 1.650T^{-1} - 7.798x10^{-3}T)x4.1868 \; kJ/mol \tag{29}$$

In this experiment, the process gas used was 4.2% H$_2$-bal Ar. The moist gas was prepared by bubbling in water at 21 °C, providing a saturated water pressure of 0.025/0.858 = 0.029 atm. Since the mole fraction of argon is invariant, the known pressures of Ar, H$_2$O, and H$_2$ in the process gas permit the calculation of the sum of p_{H_2O} and p_{H_2} as,

$$p_{H_2O} + p_{H_2} = (0.025 + 0.042 \times 0.858 \times (1-0.025)) = 0.060 \, atm \tag{30}$$

Eq. 28 and 30 may be solved simultaneously to give,

$$p_{H_2O} = \frac{0.060 K_w \sqrt{p_{O_2}}}{1 + K_w \sqrt{p_{O_2}}} \tag{31}$$

which relates the local water vapour pressure to the measured oxygen pressure. For dry gas, the prefactor in the numerator is just 0.042 x 0.858 = 0.036. The calculated p_{H_2O} for moist and dry 4.2% H$_2$-bal Ar as a function of temperature are plotted in Figure 4. Also plotted are the calibration curves for the moist and dry gas without any specimen in the process vessel. It is seen that the water vapour pressure is considerably higher when the specimen is included.

Co-Ionic Conduction in Protonic Ceramics of the
Solid Solution, BaCe$_{(x)}$Zr$_{(y-x)}$Y$_{(1-y)}$O$_{3-\delta}$ Part II: Co-Ionic Conduction
515

In the case of the calibration runs, the water vapour pressure is the same as expected from the prepared inlet gas, but with the specimen in place, the p_{H_2O} is about 50% greater for the moist case and almost 10 times greater for the dry case.
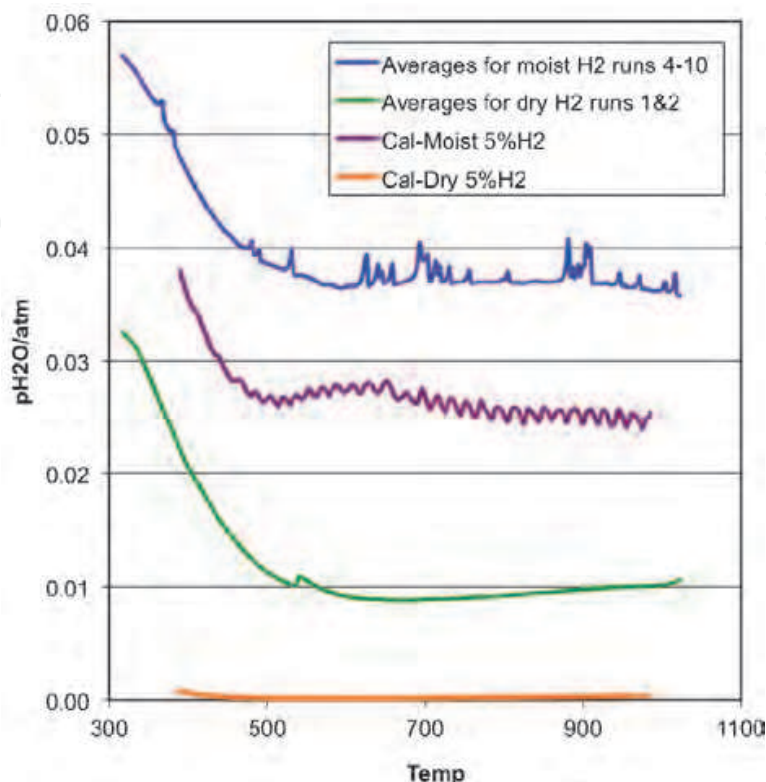

Fig. 4. Water vapor pressure for moist and dry 4.2% H$_2$-bal Ar process gas with specimen, and calibration without specimen, as calculated from the Nernst voltage of the in-situ oxygen sensor.

6.7 Isobaric conductivity measurements

Isobaric conductivity measurement requires that steady-state equilibrium of the specimen be maintained with the surrounding atmosphere so that the concentration profile of the mobile ionic species in the specimen is completely uniform. Even with the relatively thin cross-section of our rod specimens, this presented a challenge. Rapid equilibration above about 800 °C is easily achieved, but below this temperature, where most of the hydration and dehydration actually takes place, equilibration times become progressively longer because the self-diffusivities of protons and oxygen ion vacancies decrease exponentially. If the rate of change of temperature is too great, the measured conductivity does not reflect the true equilibrium defect concentration profile. This is typically observed as hysteresis in the data between increasing and decreasing temperature measurements. For these experiments impedance data for analysis was obtained under isobaric conditions upon decreasing temperature from 1030 °C to 250 °C at 0.5 °C per minute followed by rapid heating at 5 °C to the starting temperature. The experiment was repeated ten times in moist hydrogen to ensure repeatability and the absence of hysteresis effects. This extreme cyclic testing confirms the mechanical and chemical integrity of 2NiBCZY27 prepared from barium sulphate instead of barium carbonate (see Part I for details) since practically no change in conductivity was observed. Figure 5 shows an Arrhenius conductivity plot of the specimen measured in both moist and dry 4.2%H$_2$/bal Ar.

The curve for moist hydrogen represents the average for the final seven separate runs, and the curve for dry hydrogen is for the average of two runs.
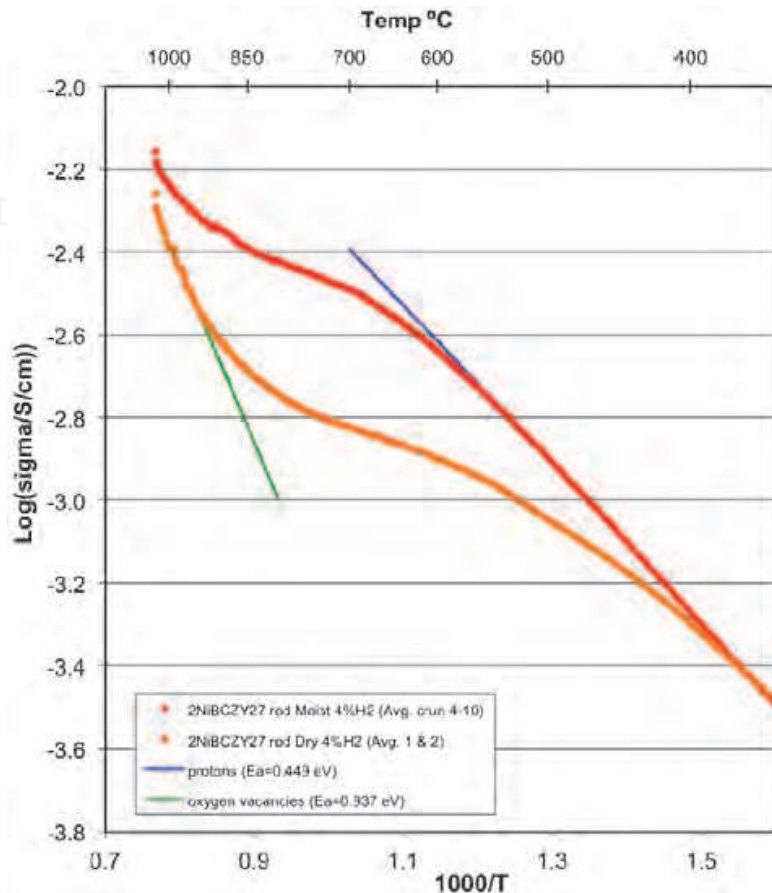

Fig. 5. Arrhenius plot of log(base 10) conductivity vs. reciprocal temperature. Upper curve is for moist and lower curve is for dry 4.2% H₂.

The curves exhibit the characteristic hydration/dehydration "crook". Below 500 °C in moist hydrogen, the specimen was assumed to be hydrated at the hydration limit of $\chi = 1$. Conductivity in this region has been attributed exclusively to protons, and the slope and intercept are indicated by a linear extension. At the highest temperature obtained in moist hydrogen, the specimen still retained substantial hydration, however, in dry hydrogen, the specimen was assumed fully dehydrated ($\chi = 0$) with conduction attributed exclusively to oxygen ion vacancies. The linear extension in this region is also shown. At the two extremes it is possible to determine the species self diffusivities using conventional Arrhenius analysis where the slope times 1000 k_B gives E_a and the y-axis intercept give the log term on the right containing the diffusion pre-exponential.

$$\ln(\sigma_{OH}T) = -\frac{E_{a,OH}}{kT} + \ln(\beta D^*_{OH}) \tag{32}$$

$$\ln(\sigma_{Vo}T) = -\frac{E_{a,Vo}}{kT} + \ln(2\beta D^*_{Vo}) \tag{33}$$

For BCZY27, the constant β evaluates to 2.403x10⁶ [K.s/Ω.cm³]. Species self-diffusivities are presented in Table 1.

Co-Ionic Conduction in Protonic Ceramics of the
Solid Solution, BaCe$_{(x)}$Zr$_{(y-x)}$Y$_{(1-y)}$O$_{3-\delta}$ Part II: Co-Ionic Conduction

517

species	D* (cm/s)	E$_a$ (eV)
Protons	3.45×10^{-4}	0.449
Oxygen ion vacancies	5.65×10^{-3}	0.937

Table 1. Measured transport parameters for protons and oxygen ion vacancies in NiBCZY27

Figure 5 highlights a common misinterpretation of Arrhenius plots in the literature. The foundation of Arrhenius analysis is based on exponentially activated diffusivity. Since, from the Nernst-Einstein equation, conductivity is proportional to the product of diffusivity and concentration, diffusivity can only be correlated with conductivity data when the species concentration is constant. The slope of an Arrhenius conductivity curve cannot be interpreted as the activation energy when the species concentrations are changing. This may be clearly seen from Eq. 16, where ln(σT) only has a meaningful slope when χ is either 0 or 1. The assumption of fixed defect concentrations in single-species ionic conductors is (usually) valid, but this is not the case with co-ionic conductors during hydration and dehydration, where concentrations of defects depend on temperature. Arrhenius analysis is only strictly valid in co-ionic conductors in the limits of total hydration and dehydration.

6.8 Data fitting to CIC model

With the species self-diffusivities determined in the previous section, it was possible to fit the total conductivity data over the intervening temperature range as a function of χ. This was done using the conductivity and in-situ water vapour measurements in moist hydrogen. A least-squares fit for Eq. 16 was obtained for hydration enthalpy and entropy as the two fitting parameters, which were -120.6 kJ/mol and -110.6 J/mol.K, respectively. This enthalpy value is slightly less negative than the value of -125 ± 2 kJ/mol obtained by TG-DSC recently reported by Ricote (Ricote, et al. 2011), and in line with the empirical curve proposed by Norby based on electronegativity of A and B-sites (Norby, 2009). The fitted entropy is close to the value of -120 J/mol K predicted by Norby based on the entropy of vaporization of water. This is by no means an assertion that the present fitted values are correct. It mostly draws attention to the difficulty in making this measurement with confidence. The scatter in reported values for enthalpy and entropy of hydration that has appeared in the literature over the years is a matter for concern. Fitting of conductivity data to give reasonable values, as reported by us, is encouraging, but may be just a happy accident. Norby's group at the University of Oslo has been making progress with this measurement lately, but the matter is far from resolved.

The hydration enthalpy and entropy values obtained by fitting the moist hydrogen conductivity data were used in an attempt to fit the dry hydrogen conductivity data, as shown in Figure 6. It is observed that, although the curve has the right qualitative features, the CIC model does not fit the dry hydrogen data very well. The upper green curve is for the CIC model prediction using the measured water vapour pressure, as presented in Figure 4. The CIC model considerably over-estimates the conductivity throughout the hydration-dehydration region. The lower blue curve is the CIC prediction using fixed p_{H_2O} = 0.0015 atm – in line with the dry hydrogen entering the process vessel. The fit is slightly better, but does not answer the obvious question why the conductivity does not reflect the measured p_{H_2O} near the specimen. Apparently defect reactions take place at low extent of hydration that compete with Wagner hydration, causing the CIC model to break down.
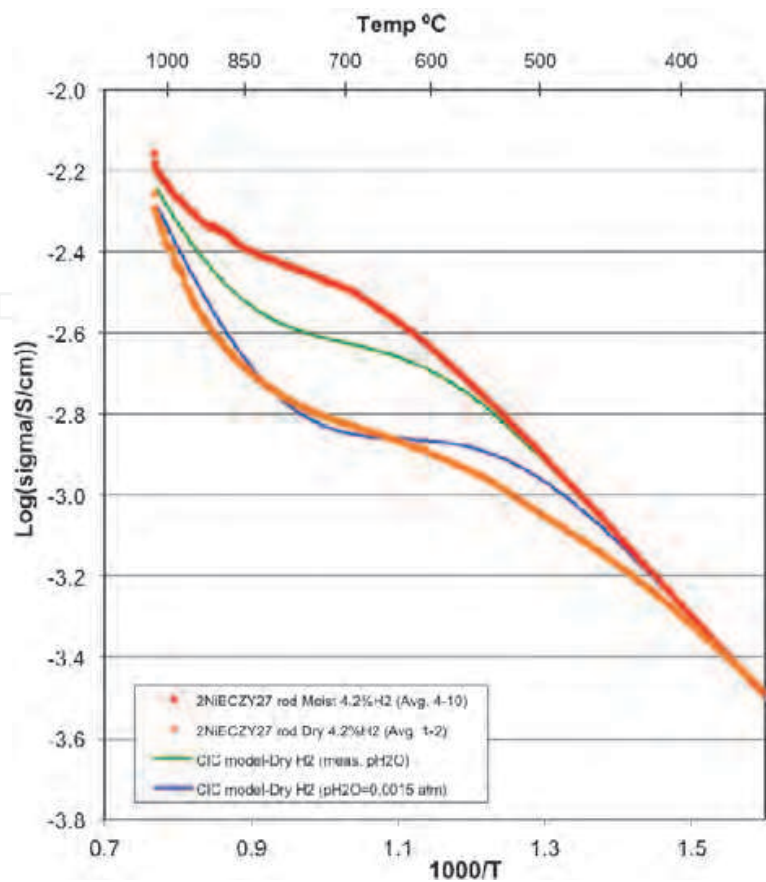
Fig. 6. Moist hydrogen data fit (red curve) with ΔH = -120.6 kJ/mol and ΔS = -110.6 J/mol.K. Failure of CIC model in dry hydrogen (orange). Green curve represents predicted values at the measured pH2O , and the blue curve, the predicted values for dry hydrogen (pH$_2$O = 0.0015 atm)

The complete conductivity plot, based on all the fitted parameters, is shown in Fig. 7. The decomposition of total conductivity into partial conductivities of protons and oxygen ion vacancies is accomplished using the Co-Ionic Conductivity model. The proton transference number refers to the right-hand axis. The figure captures the important transport features of the co-ionic ensemble. Proton conductivity reaches a maximum at 775 °C. This maximum in proton conductivity is characteristic of dehydration at higher temperatures. The peak proton conductivity for BCZY27 is 3.3 mS/cm. This relatively low conductivity value is consistent with values reported in the literature in the absence of hole conduction. Oxygen ion vacancy conductivity is greater than proton conductivity above 1000 °C, but at the peak in proton conductivity, is already about one order of magnitude lower. Oxygen ion vacancy conductivity bows downward as the concentration of vacancies decreases with decreasing temperature, and below about 500 °C the "dog leg" appears (not shown on the chart) where the residual vacancy concentration become frozen in at some small value. From the partial conductivities, the protonic transference number, t_p, was determined. At the peak in proton conductivity, t_p is only about 0.9, meaning that considerable ambipolar steam permeation is expected to occur at 740 °C. At 600 °C protonic conductivity is only slightly reduced, but t_p is 0.98. Any process that requires high selectivity for proton transport must, therefore, operate below 600 °C

Co-Ionic Conduction in Protonic Ceramics of the
Solid Solution, BaCe$_{(x)}$Zr$_{(y-x)}$Y$_{(1-y)}$O$_{3-\delta}$ Part II: Co-Ionic Conduction

519
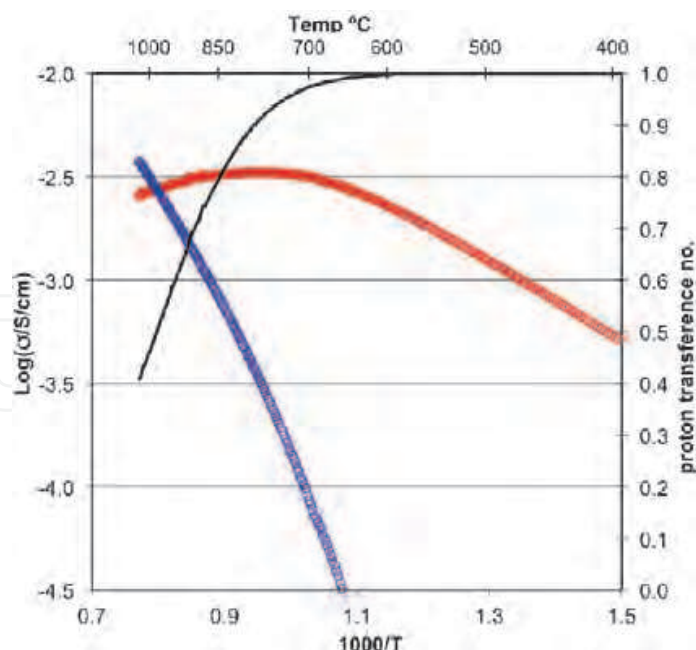
Fig. 7. Isobaric BCZY27 conductivity in moist 4.2%H$_2$/bal Ar based on CIC model. Partial conductivities are for protons (red) and oxygen vacancies (blue). Protonic transference (black) refers to right-hand axis.

7. Conclusions

Wagner hydration and Kreuer's transport models unambiguously predict that ambipolar, co-ionic conduction takes place in protonic ceramics. This has been well demonstrated by isobaric dehydration weight loss and isotope transport experiments. The co-ionic conduction model presented above is a logical extension of this transport theory that provides insight into the qualitative features of the total conductivity in Arrhenius plots that have appeared in the literature over the years – specifically, the hydration "crook" that is characteristic of these materials at intermediate temperatures. This is where proton conductivity decreases with increasing temperature due to dehydration while oxygen ion vacancy conductivity increases, both in a way that is not very intuitive without the aid of the idea of partial conductivities of the two ionic species that includes a term for the degree of hydration. An attempt has been made to justify the model quantitatively by applying it to empirical conductivity data. The CIC model with all of its underlying assumptions explains the conductivity behaviour quite well in moist hydrogen, but breaks down in dry hydrogen for reasons yet to be determined. Knowing the partial conductivities of protons and oxygen ion vacancies is a prerequisite for predicting species fluxes, which has important implications for the practical uses of these materials in steam permeable membranes, fuel cells, electrolyzers, membrane reactors, and the like. A major challenge going forward is to understand what controls hydration enthalpy and entropy and to learn how to tailor these values in practical materials for specific applications, and to gain a better understanding of the role of electronic defects.

8. Acknowledgments

9. References

Coors, W.G. (2004). Steam reforming and water–gas shift by steam permeation in protonic ceramic fuel cells. J. Electrochem. Soc., Vol.151, No.7, pp.A994-A997

Coors, W.G. and Swartzlander, R. (2005). Partial conductivity measurements in $BaCe_{0.9}Y_{0.1}O_{3-d}$ by impedance spectroscopy. Proceedings of the 26th Riso International Symposium on Materials Science: Solid State Electrochemistry, Denmark, Ed. Linderoth, et.al. pp.185-196

Coors, W.G. (2007). Protonic ceramic steam-permeable membranes. *Solid State Ionics,* Vol.178, pp.481-485

Haugsrug, R. and Norby, T. (2006). Proton conduction in rare-earth ortho-niobates and ortho-tantalates. *Nature Materials, Letters.* Vol.5, pp.193-196

Kreuer, K.-D. (1999). Aspects of the formation and mobility of protonic charge carriers and the stability of perovskite-type oxides. *Solid State Ionics*, Vol.125, pp.285-302

Kreuer, K.-D. (2003). Proton-conducting oxides. *Annu. Rev. Mater. Rev.,* Vol.33, pp.333-359

Maier, J. (2004) *Physical Chemistry of Ionic Materials – Ions and Electrons in Solids*, John Wiley & Sons, Ltd. ISBN 0-470-87076-1, England

Norby, T. (1988). EMF method determination of conductivity contributions from protons and other foreign ions in oxides. *Solid State Ionics* Vol.28-30, pp.1586-1591

Norby, T. (2009). Ch. 11: Proton Conductivity in Perovskite Oxides, In: *Fuel Cells and Hydrogen Energy/ Perovskite Oxide for Solid Oxide Fuel Cells*, T. Ishihara, Ed., Springer Science+Business Media, LLC, US, pp.217-241

Ricote, S.; Bonanos, N.; Wang, H.J.; Haugsrud, R. (2011). Conductivity, transport number measurements and hydration thermodynamics of $BaCe_{0.2}Zr_{0.7}Y_{(0.1-x)}Ni_xO_{(3-d)}$. *Solid State Ionics,* Vol.185, pp.11-17

Sanders, M. and O'Hayre, R. (2008). Co-ionic materials for steam permeation: progress report. Colorado School of Mines, 10/22/2008

Sanders, M.; Elangovan, S.; Coors, W.G.; & O'Hayre, R. (2009). Results of steam flux measurements in BZY20," 17th International Conference on Solid State Ionics, Toronto, Canada, poster abstract, p.249

Sanders, M. (2009). Examining multi-species transport in BZY20 using water isotope permeation. Masters Thesis, Colorado School of Mines

Sanders, M. and O'Hayre, R., (2010). Development of a multi-species transport space theory and its application to permeation behavior in proton-conducting doped perovskites. *J. Mater. Chem.*, Vol.20, pp.6271-6281

Schober, T and Coors, W.G. (2005). Entry and exit of water vapor in bulk ceramic proton conductors. *Solid State Ionics*, Vol.176, pp.357-362

Sutija, D.; Norby, T.; and Bjornbom, P. (1995). Transport number determination by the concentration-cell/open-circuit voltage method for oxides with mixed electronic, ionic and protonic conductivity. *Solid State Ionics*, Vol.77, p167-174

Tan, X.; Liu, S.; Li, K.; & Hughes, R. (2000). Theoretical analysis of ion permeation through mixed conducting membranes and its application to dehydrogenation reactions. *Solid State Ionics*, Vol.138, pp.149-159

Wagner, C., (1968). *Ber. Bungsenges. Phys. Chem.,* Vol.70, p.781

Yoo, H-I; Yeon, J.; & Kim, J. (2009). Mass relaxation vs. electrical conductivity relaxation of a proton conducting oxide upon hydration and dehydration. *Solid State Ionics*, Vol.180, pp. 1443-1447
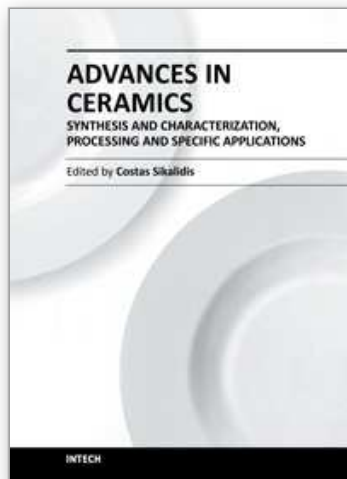
The current book contains twenty-two chapters and is divided into three sections. Section I consists of nine chapters which discuss synthesis through innovative as well as modified conventional techniques of certain advanced ceramics (e.g. target materials, high strength porous ceramics, optical and thermo-luminescent ceramics, ceramic powders and fibers) and their characterization using a combination of well known and advanced techniques. Section II is also composed of nine chapters, which are dealing with the aqueous processing of nitride ceramics, the shape and size optimization of ceramic components through design methodologies and manufacturing technologies, the sinterability and properties of ZnNb oxide ceramics, the grinding optimization, the redox behaviour of ceria based and related materials, the alloy reinforcement by ceramic particles addition, the sintering study through dihedral surface angle using AFM and the surface modification and properties induced by a laser beam in pressings of ceramic powders. Section III includes four chapters which are dealing with the deposition of ceramic powders for oxide fuel cells preparation, the perovskite type ceramics for solid fuel cells, the ceramics for laser applications and fabrication and the characterization and modeling of protonic ceramics.

INTECH
open science | open minds